

Azurin Self-Assembled Monolayers Characterized by Coupling Electrical Impedance Spectroscopy and Spectroscopic Ellipsometry

F. Bordi,[†] M. Prato,[‡] O. Cavalleri,^{*,‡} C. Cametti,[†] M. Canepa,[‡] and A. Gliozzi[‡]

INFM-CRS SOFT and Dipartimento di Fisica, Università di Roma "La Sapienza", Rome, Italy, and INFM and Dipartimento di Fisica, Università di Genova, Genoa, Italy

Received: June 30, 2004; In Final Form: September 28, 2004

We present a combined study of azurin monolayers deposited on both bare and hexadecanethiol-covered gold surfaces carried out by coupling two independent techniques, in situ electrical impedance spectroscopy (EIS) and ex situ spectroscopic ellipsometry (SE). The combination of the two techniques which probe different sample properties in different environmental conditions results in a cross-consistent characterization of the optical and electrical properties of the protein layers. Moreover, it provides a reliable estimate of the layer thickness. Azurin self-assembles on bare gold forming a monolayer with a thickness of 3.2 ± 0.2 nm, a value very close to the crystallographic height of the cylindrically shaped protein. When azurin is deposited on hexadecanethiol-covered gold, a protein layer thickness of 2.7 ± 0.2 nm is obtained. This indicates that azurin forms a less dense layer when it is deposited on thiol-covered gold compared to the adsorption on bare gold. Both EIS and SE provide a direct estimate of the dielectric constant of the protein layer in the hydrated and dry states, respectively. In the case of the composite azurin/hexadecanethiol system, the combined EIS and SE analysis proves to be a valuable tool for the correct interpretation of the EIS data and allows for an estimate of the azurin and hexadecanethiol conductivity ratio.

1. Introduction

Supramolecular assemblies are attracting increasing interest both on fundamental and applicative ground.^{1,2} On one hand, they allow studies on intermolecular interactions. On the other hand, the possibility of tailoring the functional properties of the exposed interface paves the way to new developments in the field of molecular devices based on properties, such as molecular recognition, enzymatic activity, or electron transfer.^{3–6} Recently, a strong interest arose on the adsorption of metalloproteins on conductive supports.^{7–10} The bottleneck in producing self-assembled monolayers (SAMs) of complex biomolecules endowed with specific functions is related to the capability of retaining the molecular functionalities upon adsorption. In this respect, direct interaction with inorganic hard surfaces may be destructive. The insertion of a soft spacer layer, such as alkanethiol or silane SAMs or supported bilayers, is a viable strategy to biomolecule/substrate uncoupling.^{11–15} A good immobilization method should produce stable biomolecule anchoring and reproducible molecular packing, resulting in a fine-tuning of layer coverage and thickness.

We shall focus here on azurin, a blue copper protein of a molecular weight of 14 kDa consisting of 128 residues, and compare the properties of azurin layers deposited on both bare and hexadecanethiol-covered gold surfaces. Azurin is a metalloprotein which acts as an electron-transfer agent in the respiratory chain of denitrifying bacteria, where it transports electrons between cytochrome *c*₅₅₁ and cytochrome oxidase. It has been shown, by means of differential pulse voltammetry and EIS, that azurin can retain its electron transfer properties also after adsorption on surfaces.¹⁶ Moreover the apparent rate constant of the process was determined for azurin adsorbed both

on bare¹⁶ and on hexanethiol covered gold.¹⁷ Attempts toward the realization of biomolecular electronic devices based on immobilized azurin have recently been proposed.¹⁸ The demand for stable and reproducible devices prompts the careful investigation of the SAM molecular structure. The layer thickness, which depends on molecular density and orientation, is a key point to understand SAM functional properties such as electron-transfer mechanisms. In a previous work we characterized the morphology of azurin layers on bare and thiol covered gold surfaces by means of scanning probe microscopy.¹⁹ From AFM inspection of the azurin/thiol interface, a submonolayer protein coverage with an estimated protein height of about 4 nm was inferred. In the case of azurin adsorption on bare gold, different coverage values have been reported depending on the protein deposition protocol.¹⁶ An effective layer thickness much lower than the protein size, suggesting a low fractional coverage, has been reported for azurin layers deposited both on gold and functionalized silicon oxide surfaces.²⁰ The choice of substrate and the deposition protocol are therefore crucial to the resulting layer properties.

Here, we present a combined study of the protein layer which couples two independent techniques, in situ electrical impedance spectroscopy (EIS) and ex-situ spectroscopic ellipsometry (SE). EIS, which probes the sample properties in the radiowave frequency region, is a very sensitive technique to investigate the properties of biomolecule-functionalized electrodes, owing to the large effects that even small disordered or defect-containing area fractions produce on the measured electrical parameters.^{21–23} Cross-fertilization can be gained by coupling EIS results with SE data obtained in the optical wavelength range. SE is a well-established technique to get nondestructive information on the thickness and refractive index of thin films,²⁴ with sounding applications to organic and biological films.^{25,26} In this study, we exploit this experimental approach to determine both the structural features of the azurin SAMs (both on bare

* To whom correspondence should be addressed.

[†] Università di Roma "La Sapienza".

[‡] Università di Genova.

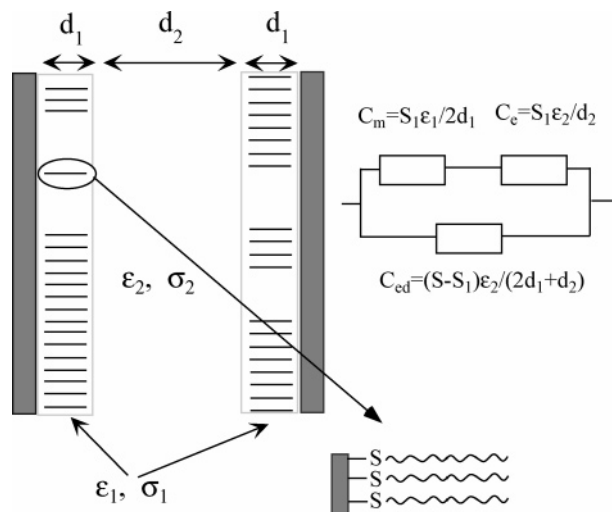


Figure 1. A sketch of the measuring cell. The system behaves as a plane parallel capacitor filled with three dielectric slabs. The electrical parameters of the monolayer and the electrolyte solution are the permittivities ϵ_1 and ϵ_2 and the electrical conductivities σ_1 and σ_2 , respectively. The capacitances C_m , C_{ed} , and C_e correspond to the electrode region covered by the adsorbed monolayer, the region covered by defects, and the bulk electrolyte contribution, respectively. The drawing is out of scale.

and hexadecanethiol-covered gold) and the electrical properties such as dielectric constant and conductivity. The determination of protein dielectric properties is a key problem that currently limits the accuracy and reliability of structure-based calculations of electrostatic energies with continuum approaches.²⁷ Moreover, recent studies on the functional role of channel proteins raised new interest for the determination of the protein dielectric constant.²⁸

2. Methods

2.1. Impedance Spectroscopy. To define a structural model for the supported monolayer, the measuring cell, whose electrodes act as support for the protein adsorption, was modeled as a parallel plane capacitor composed of three dielectric slabs, as in the sketch shown in Figure 1. The total impedance of the equivalent circuit is determined by the series of RC networks, taking into account the contribution of the monolayers at the electrode-electrolyte interfaces (capacitance C_m) and the bulk electrolyte (capacitance C_e), respectively. Defects in the monolayer were accounted for by introducing a further RC network of which the capacitance is determined by the area S_1 of the defect-free monolayer, exhibiting a capacitance C_m , and by the area $(S - S_1)$ of the electrode covered with defects, exhibiting a capacitance C_{ed} . These defects may be disordered areas with high conductivity, probably related to the surface roughness of the metal electrode. From a dielectric point of view, within the effective medium approximation theory, the system gives rise to an interfacial polarization resulting in an effective complex dielectric constant $\epsilon_{eff}^*(\omega)$ for the whole system given by

$$\epsilon_{eff}^*(\omega) = \epsilon_2^*(\omega) \frac{(2rd_1 + d_2)\epsilon_1^*(\omega) + 2(1-r)d_1\epsilon_2^*(\omega)}{[2d_1\epsilon_2^*(\omega) + d_2\epsilon_1^*(\omega)]} \quad (1)$$

where d_1 and d_2 are the thicknesses of the adsorbed monolayer and the bulk electrolyte solution, of which the permittivity and electrical conductivity are given by ϵ_1 , σ_1 , ϵ_2 , σ_2 , respectively. $r = S_1/S$ is the ratio of the electrode surface covered by the monolayer to the total electrode surface. If one assumes that

the dielectric and conductometric properties of each dielectric medium can be characterized by a frequency dependence of the type

$$\epsilon^*(\omega) = \epsilon + \frac{\sigma}{i\epsilon_0\omega} \quad (2)$$

eq 1 results in a dielectric behavior described by

$$\epsilon^*(\omega) = \epsilon_\infty + \frac{\epsilon_s - \epsilon_\infty}{1 + (i\omega\tau)} - i \frac{\sigma_0}{\epsilon_0\omega} \quad (3)$$

where $\Delta\epsilon = \epsilon_s - \epsilon_\infty$ and τ are the dielectric increment (the strength of the dielectric relaxation) and the relaxation time, respectively; ϵ_s and ϵ_∞ are the low and high-frequency limits of the real part of permittivity $\epsilon'(\omega)$, and σ_0 is the dc ionic conductivity.

In the limit $d_1/d_2 \ll 1$,

$$\Delta\epsilon = \epsilon_s - \epsilon_\infty = \frac{2d_1[r d_2(\epsilon_1\sigma_2 - \epsilon_2\sigma_1)^2 + 2(1-r)d_1\epsilon_1\epsilon_2\sigma_2^2]}{\epsilon_1(2d_1\sigma_2 + d_2\sigma_1)^2} \quad (4)$$

$$\epsilon_\infty = \frac{\epsilon_2[(2rd_1 + d_2)\epsilon_1 + 2(1-r)d_1\epsilon_2]}{(2d_1\epsilon_2 + d_2\epsilon_1)} \quad (5)$$

$$\tau = \frac{\epsilon_0(2d_1\epsilon_2 + d_2\epsilon_1)}{(2d_1\sigma_2 + d_2\sigma_1)} \quad (6)$$

The characteristic properties of the monolayer (i.e., its permittivity ϵ_1), the conductivity σ_1 , and the thickness d_1 can be properly evaluated from the dependence of eqs 4–6 on the conductivity σ_2 of the electrolyte solution by means of a nonlinear least-squares fitting procedure. A similar analysis could be carried out using the relationships derived from the electrical conductivity dispersions. In particular, from the low-frequency limit σ_0 of the electrical conductivity, the parameter r can be properly evaluated in the limit $d_1/d \ll 1$ through the simple relation

$$r = \frac{\sigma_0 - \sigma_2}{\sigma_2(\sigma_1 - \sigma_2)} \left(\frac{d}{d_1} \sigma_1 + \sigma_2 \right) \quad (7)$$

where d is the distance between the two bare electrodes.

2.2. Spectroscopic Ellipsometry. SE measures the change of the light polarization upon reflection at an interface.²⁴ With reference to the incidence plane, defined by the direction of the beam and the normal to the surface, the change of the polarization state of the incident light is induced by the change of the phase and amplitude of the p (in the plane of incidence) and s (perpendicular to the plane of incidence) components of the incidence radiation. According to the Jones formalism, the reflection properties of a sample are described by the matrix:

$$\begin{pmatrix} r_{pp} & r_{ps} \\ r_{sp} & r_{ss} \end{pmatrix} \quad (8)$$

where $r_{i,j}$ are the complex reflection Fresnel coefficients. In the case of isotropic materials or materials with uniaxial anisotropy

and the optical axis perpendicular to the surface, the Jones matrix is diagonal:

$$\begin{pmatrix} r_{pp} & 0 \\ 0 & r_{ss} \end{pmatrix} \quad (9)$$

where r_{pp} and r_{ss} are the reflection coefficients for p-light and s-light, respectively. Ellipsometry measures the complex ratio $\rho = r_{pp}/r_{ss}$, traditionally expressed in terms of two angles Ψ and Δ , according to the relation:

$$\rho = \tan \Psi \exp(i\Delta) \quad (10)$$

Variable-angle SE measures ρ as a function of the wavelength and angle of incidence. Because it measures the ratio between r_{pp} and r_{ss} , SE is very accurate, and no calibration with a reference material is necessary. Further, the parameter Δ , describing a phase quantity, displays enhanced sensitivity to the presence of very thin films, down to the monolayer level. Note that SE does not directly measure the optical functions and thickness of the examined sample. The latter quantities can be obtained from SE measurements by fitting the experimental data with simulations based on a suitable optical model of the system under consideration. The simplest simulations are usually based on isotropic multilayered structures separated by sharp interfaces. Each layer of the stack is characterized by an optical function $N_j(\lambda) = (n_j(\lambda), k_j(\lambda))$, where $n_j(\lambda)$, $k_j(\lambda)$ are the real and imaginary parts of the complex index of refraction. $n_j(\lambda)$, $k_j(\lambda)$, and the effective thickness d_j can be assumed as a free parameter, to be varied until the best agreement between data and calculations is reached through minimization of the so-called mean-squared error or other convenient likelihood parameter. In particular cases, especially when relatively thick films with reasonably known optical functions are considered, morphological parameters, such as interface mixing and roughness, film homogeneity, thickness uniformity, or concentration gradient, can be also inferred.

In the case of transparent layers of nanometric thickness, such as those considered in this paper, a correlation exists between the refractive index and thickness which imposes further approximations in the analysis. Therefore, a reliable determination of the thickness requires some a priori knowledge of the optical functions and morphological properties of the films.

3. Experimental Section

3.1. Materials. cDNA of azurin was a generous gift of A. Desideri. The protein was expressed and purified as detailed elsewhere.¹⁹ Hexadecanethiol (hereafter referred to as C16) (purity $\geq 97\%$), ethanol (purity 98%), HClO_4 (70%), and ammonium acetate (AcONH_4 , 5 M BioChemika MicroSelect) were purchased from Fluka and used as received. Inorganic salts (ACS grade) used to prepare electrolyte solutions were obtained from Aldrich and used without further purification. AcONH_4 buffer (50 mM, pH = 4.6) was prepared from a 5 M stock solution, and the pH was adjusted with HClO_4 to the final value. The deposition of alkanethiol and azurin SAMs was performed in 1 mM alkanethiol solution in ethanol and 10 μM azurin solution in ammonium acetate buffer, respectively.

3.2. Sample preparation. Gold electrodes for EIS measurements were prepared by vacuum evaporation of 120–150 nm gold (99.999% purity) (Corradi, Italy) onto freshly cleaved mica sheets. The evaporation was carried out at a base pressure of $2 \cdot 10^{-6}$ mbar. The substrate temperature was kept at 650 K. The deposited films were then annealed in situ for 1–2 h at the same temperature. Before mounting in the EIS measuring cell,

the samples were annealed in a butane flame to red glowing and quenched in ethanol. Scanning tunneling microscopy inspection of the flame-annealed films showed atomically flat (111) terraces, with a typical size of a few hundred nanometers, displaying the herringbone reconstruction.¹⁹ The procedure adopted to deposit SAMs for EIS measurements can be summarized as follows: First, the measuring cell was filled with an electrolyte solution of known molarity (NaCl, in the range 10^{-4} – 10^{-2} mol/L). Dielectric and conductometric measurements were performed in the whole frequency range investigated (from 40 Hz to 100 MHz). Spectra were characterized by a permittivity $\epsilon(\omega)$ dominated by the electrode polarization effect that, in the low-frequency range, is well described by a power law $\epsilon(\omega) \approx \omega^{-\gamma}$ with a typical exponent on the order of 0.7–0.8, depending on the ionic strength. The electrolyte solution was then removed and substituted with the appropriate solution containing the molecules to be deposited. The formation of the monolayer was assumed complete when the electrical impedance of the measuring cell (modulus and phase angle of the electrical impedance) reached a steady-state value. Kinetics of the monolayer formation were in the range of hours, which was acceptable for practical use. After solution removal, the cell was refilled with the NaCl electrolyte solution, and the newly recorded dielectric and conductometric spectra were compared to those obtained before the monolayer formation. A new relaxation region located at frequencies on the order of 100 kHz was detected either in the permittivity $\epsilon'(\omega)$ or electrical conductivity $\sigma(\omega)$ and attributed to the formation of the SAM. This experimental procedure allowed us to measure the effects associated with the molecules adsorbed at the electrode surface, neglecting their bulk contribution. Alkanethiol- and azurin-covered gold interfaces exhibited good stability, as no apparent changes in the overall dielectric spectra were observed over at least 1 day after the adsorption process was completed.

In the case of SE measurements, gold films deposited on Cr-primed borosilicate glass slides (Arrandee, denoted as Au_g in the following text) were preferred to films grown on mica sheets. Au_g films are, in fact, very homogeneous from the optical point of view. Similarly to samples used for EIS, the substrates were flame-annealed and incubated in the self-assembly solution immediately after an SE quality check. The optical properties of the films derived from SE characterization after flame annealing gave results in excellent agreement with the literature on high-quality, flat gold films.^{30,31} We note that Aspnes et al. pointed out the importance of surface roughness in affecting the determination of the optical constant of metal films (in particular, gold).³⁰ In this respect, we compared our data on freshly annealed gold surfaces with recent model calculations of gold optical constants as a function of roughness.³² The values of Δ at 70° and at $\lambda \approx 632$ nm that we obtained on about 20 bare substrates showed a narrow distribution around $\sim 109.5^\circ$. This value matches the value of 109.4° calculated for a flat surface and is much larger than the value (106°) calculated in the case of a root-mean-squared roughness of 5 nm.³² These observations correlate rather well with the results of an AFM inspection (Multimode, Digital Instruments, Santa Barbara, California) which indicate a roughness of about 3 nm over $10 \times 10 \mu\text{m}^2$. The good quality of the flame-annealed film can be also figured out by depolarization measurements. The depolarization of Au_g substrates was $< 1.5\%$ for $\lambda > 300$ nm, increasing (but always below 5%) toward the UV limit of the spectrum. We finally observed that the SE check of substrates involved a limited exposure to atmospheric contamination. We measured a typical decrease of Δ of $\sim 0.03^\circ$ after 300 s. This decrease is

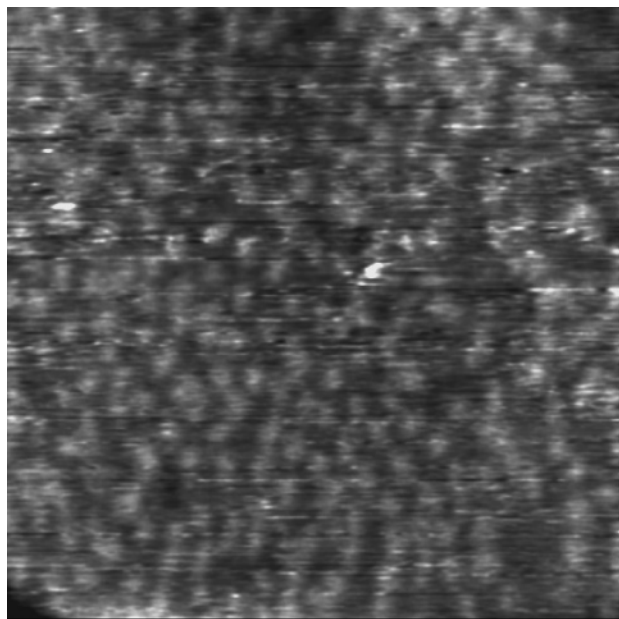


Figure 2. STM image of the azurin/gold interface. Image size: 44 nm \times 44 nm. Tunneling parameters: 2.8 nA, 310 mV.

equivalent to the formation of a layer of contaminants with an effective thickness of about 30 pm. SAM deposition was accomplished by overnight immersion of Au_g substrates into appropriate solutions at room temperature. SE measurements were performed immediately after extraction, accurate rinsing with solvent, and drying under nitrogen flow. Ex situ STM inspection (Digital Instruments, Santa Barbara, California) of an azurin layer self-assembled on a gold film deposited on mica indicates the formation of a fairly uniform protein layer as shown in Figure 2.

3.3. Dielectric measurements. Dielectric and conductometric measurements have been carried out in the frequency range from 40 Hz to 100 MHz, by means of frequency-domain dielectric spectroscopy using a Hewlett-Packard Impedance Analyzer model 4294A. All measurements have been carried out at the temperature of 25 °C. The input admittance $Y(\omega)$ of the measuring cell has been converted to the complex dielectric constant $\epsilon^*(\omega)$ on the basis of an appropriate electrical network which represents the electrochemical system, of which the constants have been determined by calibration using liquids of known permittivity and conductivity. In the whole frequency range, the overall accuracy of the measurements is within 2% on the permittivity and less than 1% on the conductivity of the investigated system. The dielectric cell comprises a Perspex body and a spacer limiting the area of the gold electrodes and supporting two plane electrodes 2 mm apart. The volume of the cell is about 0.8 mL.

3.4. Spectroscopic Ellipsometry Measurements. SE measurements were performed on a rotating compensator spectroscopic ellipsometer (M-2000, J. A. Woollam Co., Inc.), which allows for simultaneous measurements at 225 wavelengths in the range 245–725 nm. The instrument was tested on Si wafer standards and on cadmium stearate Langmuir–Blodgett films.³³ In the present work, spectra have been collected at incidence angles in the 60–70° range. Calculations and fitting to data were performed using the software supplied by the manufacturer (WVASE32, J. A. Woollam Co., Inc.).

4. Results

4.1. Impedance Spectroscopy. The dielectric and conductometric spectra in the low-frequency region are affected by a large parasitic effect, known as the electrode polarization effect, because of the relatively high value of ionic conductivity of the electrolyte solutions used. Also, in electrode regions covered by the much less conductive monolayer, the space charge close to the electrolyte interface leads to an ionic double layer, and a further contribution to the electrode polarization is expected.³⁴

This effect is due to an accumulation of spatial charge at the metal–electrolyte interface that strongly modifies the electrical behavior of the whole system.³⁵ In the present case, the electrode polarization contribution has been described, within the constant phase angle (CPA) model, by an electrical admittance of the form

$$Y_p(\omega) = K(i\omega)^\alpha \quad (11)$$

where K is a parameter depending on the electrical conductivity and $0 \leq \alpha \leq 1$. The equivalent circuit modeling the measuring cell can be represented by an admittance $Y_s(\omega)$ (a parallel combination of a resistance R_s and a capacitance C_s) in series to the admittance $Y_p(\omega)$; the measured complex dielectric constant $\epsilon_m^*(\omega)$ is then given by

$$\epsilon_m^*(\omega) = \frac{1}{i\omega C_0} \frac{Y_s(\omega)}{1 + \frac{Y_s(\omega)}{Y_p(\omega)}} = \frac{\epsilon^*(\omega)}{1 + \frac{C_0(i\omega)^{1-\alpha}}{K} \epsilon^*(\omega)} \quad (12)$$

where $\epsilon^*(\omega) = \epsilon'(\omega) - i\epsilon''(\omega)$ is the effective complex dielectric constant of the sample to be investigated, $C_0 = \epsilon_0 S/l$ is the geometric capacitance of the measuring cell (for an equivalent plane parallel cell, S is the surface and l the electrode distance), ϵ_0 is the dielectric constant of free space, and ω is the angular frequency of the applied electric field.

A nonlinear least-squares regression can be used to determine the parameters of the electrode polarization effect (the exponent α and the prefactor K) and the parameters describing the frequency dependence of the complex dielectric constant $\epsilon^*(\omega)$, according to the chosen relaxation function reported in eq 3.

Typical dielectric and conductometric spectra obtained in NaCl electrolyte solutions before and after the SAM formation on the gold electrode are shown in Figures 3 and 4 in the case of C16 and azurin, respectively. As can be seen, in both cases, a new dielectric relaxation region, depending on the electrolyte concentration, appears that strongly modifies the dielectric behavior of the whole system. The same behavior is observed in the case of azurin adsorption on C16-covered gold electrodes. Figure 5 shows typical dielectric spectra for two different electrolyte concentrations, where the behavior of the untreated electrode is also shown for comparison. Also, in this case, a marked dielectric relaxation appears.

The presence of electrode polarization effects, giving rise to a relaxation that partially overlaps to the relaxation to be evidenced, makes the deconvolution of the spectra a very difficult task. This difficulty is particularly severe in the case of high electrical conductivity of the system, resulting in a contribution to the total dielectric loss which is orders of magnitude larger than that associated with the presence of the adsorbed monolayer. To overcome this difficulty, we have performed a multistep fitting procedure based on the Marquardt algorithm for a complex function.³⁷ Because the shape of the dielectric loss spectrum strongly depends on the value of the

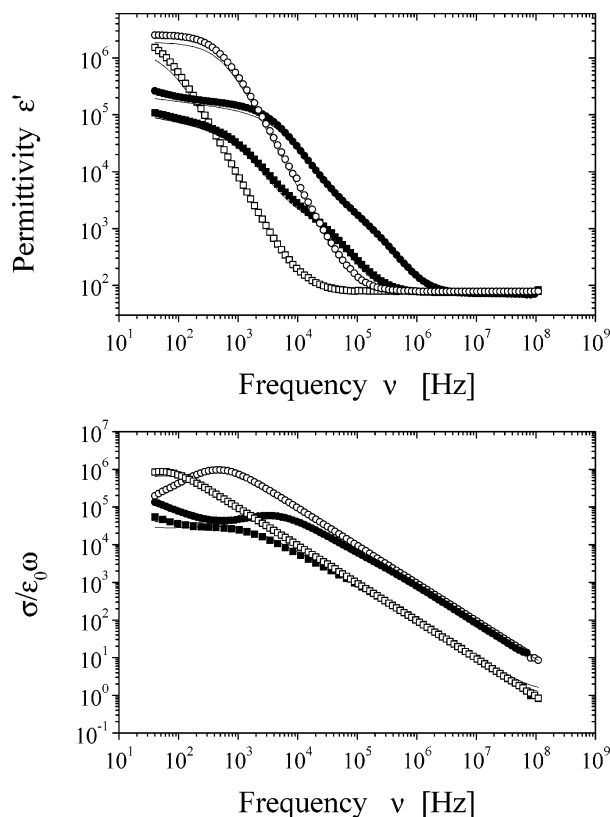


Figure 3. Dielectric (top) and conductometric (bottom) spectra measured in NaCl electrolyte solutions at two different concentrations in the absence (open symbols) and presence of hexadecanethiol monolayer on the gold electrode. (□) and (■): $5 \cdot 10^{-4}$ mol/L; (○) and (●): $5 \cdot 10^{-3}$ mol/L. The full lines are the calculated values according to the fitting procedure employed.

dc electrical conductivity σ_0 to be subtracted from the total loss $\sigma(\omega)/\epsilon_0\omega$, we made a preliminary simultaneous fit of ϵ' and the total loss $\sigma(\omega)/\epsilon_0\omega$ with four free parameters $\Delta\epsilon$, τ , ϵ_∞ , and σ_0 . The value of σ_0 thus obtained was then subtracted from the measured conductivity $\sigma(\omega)$, the dielectric loss was again evaluated, and a new set of parameters from the simultaneous fit of both the permittivity $\epsilon'(\omega)$ and the electrical conductivity $\sigma(\omega)$ was obtained. This procedure was iterated until a minimization was reached.

The results are shown in Figure 6, where the dielectric increment $\Delta\epsilon$ and the relaxation time τ are plotted as a function of the NaCl electrolyte concentration for all of the systems investigated. The electrical parameters of the monolayers were determined by a nonlinear least-squares fit of eqs 4 and 6 to the values derived from the analysis of the dielectric spectra reported in Figure 6. The minimization is based on four adjustable parameters, ϵ_1 , σ_1 , d_1 , and r , reflecting the electrical and geometrical properties of the adsorbed monolayer. The overall accuracy is within 5–10% for all the parameters, with the exception of the monolayer conductivity σ_1 , whose estimation, although of the correct order of magnitude ($\sigma_1 \approx 10^{-6}$ – $10^{-7} \Omega^{-1} \text{ m}^{-1}$), is less accurate.

EIS indicates a monolayer thickness of 2.3 ± 0.2 nm and 3.2 ± 0.2 nm for C16 and azurin SAMs, respectively (Table 1). A more careful data analysis is needed in the case of the azurin/C16 system. In this case, a simple model which treats the double-layered film as a single effective layer is too crude and leads to a significant underestimation of the film thickness. As will be discussed in the following text, in this case, the

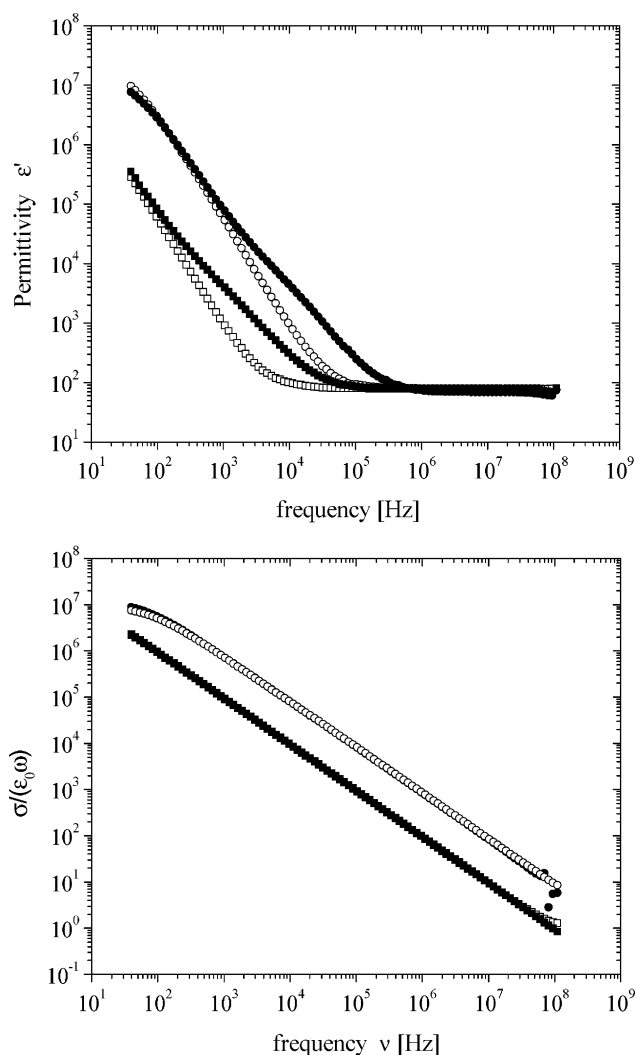


Figure 4. Dielectric (top) and conductometric (bottom) spectra measured in NaCl electrolyte solutions at two different concentrations in the absence (open symbols) and presence of an azurin layer on the gold electrode (full symbols). (□) and (■): $5 \cdot 10^{-4}$ mol/L; (○) and (●): $5 \cdot 10^{-3}$ mol/L. The full lines are the calculated values according to the fitting procedure employed.

combined EIS and SE analysis proved to be a valuable tool for the correct interpretation of the EIS data.

As concerns the permittivity data, ϵ_1 of the C16 monolayer is about 2.35, while a higher ϵ_1 value, $\epsilon_1 = 2.85$, is obtained for azurin. As concerns the azurin/C16 system, an intermediate value $\epsilon_1 = 2.5$ is found (Table 1).

For all of the systems investigated, coverage was evaluated by both the nonlinear least-squares fit of eqs 4 and 6 and from eq 7, which in the limit $\sigma_2 \gg \sigma_1$ reduces to $\sigma_0 \approx \sigma_2(1 - r)$. The two methods gave similar results showing a slight sample-to-sample variability in the estimated coverage, with a value ranging from 0.7 to 0.8.

This value is a reasonable surface coverage for protein layers and is in agreement with results previously reported.¹⁶ In the case of alkanethiol SAMs, on the basis of a number of structural investigations,³⁸ well-ordered and insulating monolayers are formed on Au. The low coverage obtained here is likely related to the deposition protocol used for EIS experiments, which involved air exposure of the bare gold substrates during cell mounting. In fact, SE experiments, which involved a shorter air exposure of the substrates, resulted in the formation of high-coverage SAMs (see text to follow).

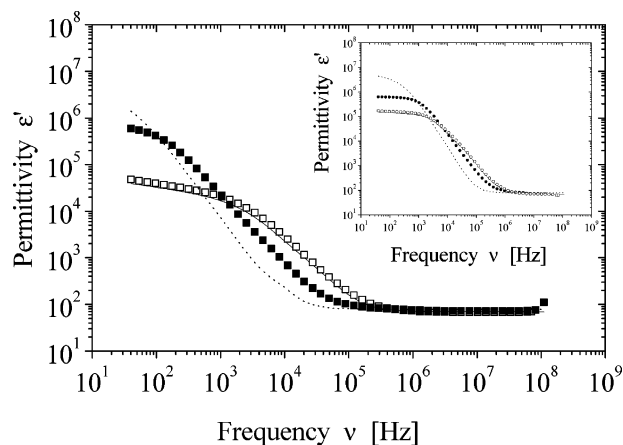


Figure 5. Dielectric spectra measured in $5 \cdot 10^{-4}$ mol/L NaCl solutions in the absence (dotted line) and presence of an azurin layer (full symbols) on a pretreated gold electrode, on which a hexadecanethiol monolayer was self-assembled (open symbols). The inset shows the dielectric behavior at a different electrolyte concentration, $5 \cdot 10^{-3}$ mol/L. The full lines are the calculated values according to the fitting procedure employed.

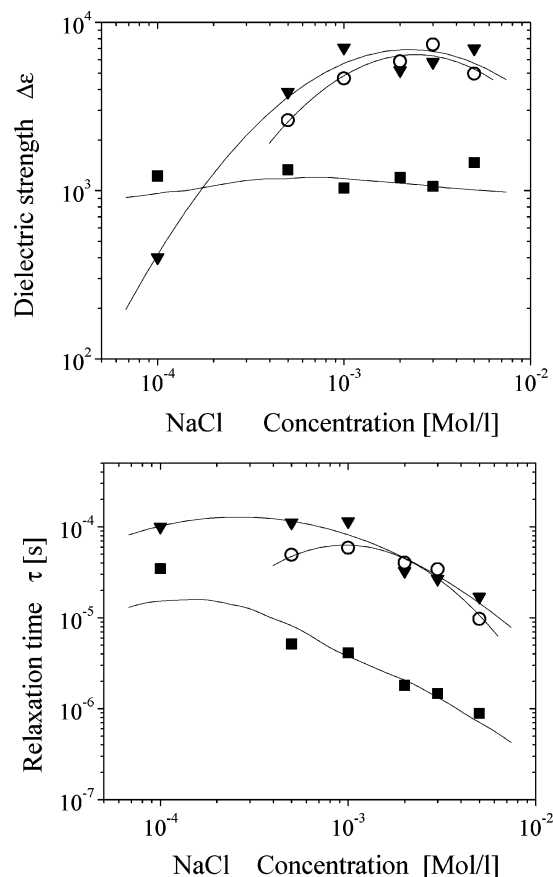


Figure 6. The dielectric increment $\Delta\epsilon$ (top) and the relaxation time τ (bottom) as functions of NaCl concentration, measured with electrodes covered with different monolayers: (▼), azurin; (■), hexadecanethiol; (○), azurin on a hexadecanethiol pretreated electrode. The full lines are the values derived from the fitting procedure (eqs 4 and 6).

4.2. Spectroscopic Ellipsometry. Representative SE spectra obtained at 65° angle of incidence on adsorbate-covered samples are shown in Figure 7 together with spectra collected on corresponding bare substrates. The data taken on a single sample were characterized by an extremely high repeatability. Limited variability was observed over the different samples. The data are therefore presented after averaging over the whole ensemble

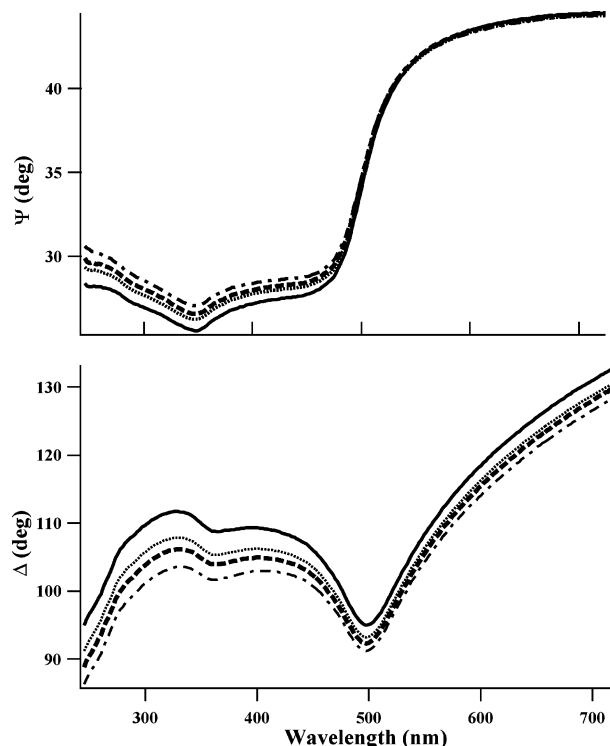


Figure 7. Ψ and Δ spectra obtained on bare substrate (solid lines) and on hexadecanethiol (···), azurin (---), and azurin/hexadecanethiol (- · -) covered gold substrates.

of samples (about 10 for each species considered). For such ultrathin layers, the decrease of Δ can be assumed roughly proportional to the layer thickness d_{SAM} . Qualitative inspection of SE spectra suggests, therefore, that $d_{\text{hex}} < d_{\text{azu}} < d_{\text{azu/hex}}$, as expected.

To emphasize the subtle SAM-induced changes of SE patterns, difference spectra $\delta\Psi = \Psi_{\text{SAM/Au}} - \Psi_{\text{Au}}$ and $\delta\Delta = \Delta_{\text{SAM/Au}} - \Delta_{\text{Au}}$ are reported in Figures 8 and 9, respectively.

We first examined the data obtained on C16 SAMs. In the simplest approach, the organic layer was assumed to be homogeneous and compact, a good approximation in view of the extensive experimental work performed on alkanethiol SAMs.³⁸ A crude two-phase model (SAM/Au), with abrupt interfaces, was considered, and the SAM optical properties were simulated within the so-called Cauchy approach:

$$n_{\text{SAM}} = A + \frac{B}{\lambda^2}, \quad k_{\text{SAM}} = 0$$

where the light wavelength is expressed in μm and the coefficients A and B were used as adjustable parameters.

For C16 data, a minimum could be reached in the regression procedure with $A = 1.48 \pm 0.02$, $B = 5 \cdot 10^{-5} \pm 5 \cdot 10^{-5} \mu\text{m}^2$, and $d_{\text{hex}} = 2.15 \pm 0.05$ nm. The thickness/index-of-refraction correlation explains the large fit uncertainty on A and the substantial indetermination of B . The reported uncertainties indicate the 90% level of confidence. The fit uncertainty is, therefore, small in comparison to the error related to the dispersion of measurements which can be quantified in ± 0.2 nm.

The $\delta\Psi$ and $\delta\Delta$ patterns calculated according to the Cauchy model are represented as dotted curves in Figures 8 and 9, respectively. The substantial agreement regarding the Δ patterns gave confidence on the value of the thickness. However, the fit of the $\delta\Psi$ patterns is rather qualitative, reflecting the crudeness of the abrupt interface model. Therefore, as a second-step

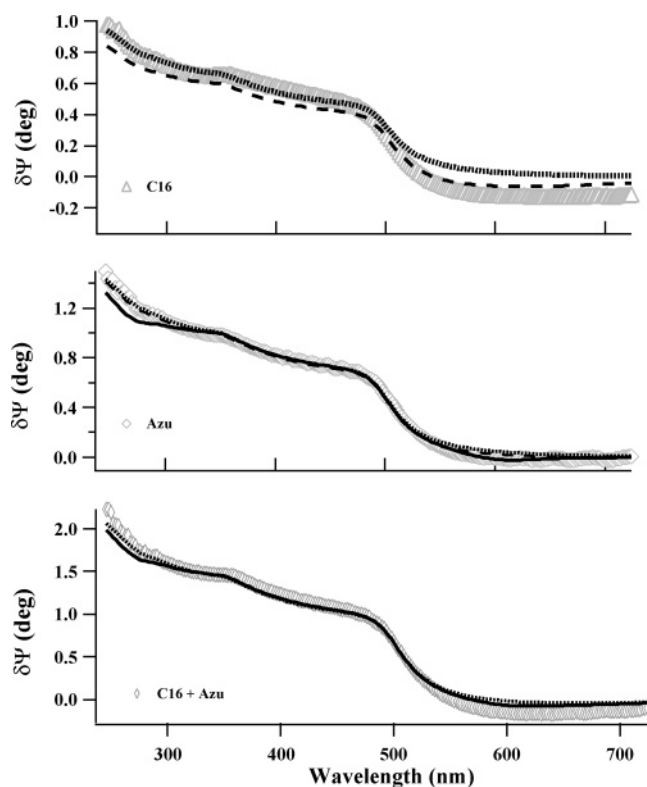


Figure 8. Difference spectra ($\Psi_{\text{SAM/Au}} - \Psi_{\text{Au}}$) from experimental data (Δ , hexadecanethiol; \diamond , azurin; \diamond , azurin/hexadecanethiol) and from generated data obtained using Cauchy model (\cdots), Lorentz model ($-$), and EMA approach ($- -$).

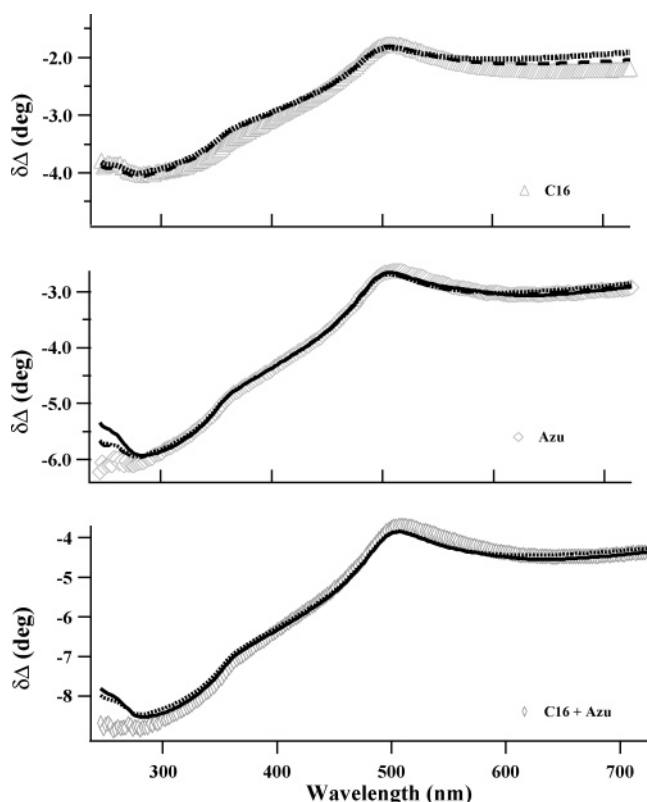


Figure 9. Difference spectra ($\Delta_{\text{SAM/Au}} - \Delta_{\text{Au}}$) from experimental data (Δ , hexadecanethiol; \diamond , azurin; \diamond , azurin/hexadecanethiol) and from generated data obtained using Cauchy model (\cdots), Lorentz model ($-$), and EMA approach ($- -$).

approximation, we considered a three-phase model (SAM/interface/Au). Following Arwin and co-workers, the optical

properties of the organic/metal interface were calculated as a weighted average of the optical properties of the substrate and the film, under the so-called Bruggeman scheme.⁴⁰ This effective medium approximation (EMA) aims to describe the interface in a less abrupt way than in a two-phase model. Furthermore, it accounts, to some extent, for the presence of domains with less dense molecular packing, disordered patches, or even empty areas.

The EMA model introduces new parameters such as the thickness of the interfacial layer, d_{int} , and f_{Au} and f_{SAM} , the gold and film volume fractions ($f_{\text{Au}} + f_{\text{SAM}} = 1$).

The SAM was modeled through the Cauchy approximation found in the two-phase analysis. The film thickness was denoted as d'_{hex} . The regression procedure on the C16 film gave $d'_{\text{hex}} = 1.75 \pm 0.05$ nm and $d_{\text{int}} = 0.35 \pm 0.05$ nm with $f_{\text{hex}} = 89 \pm 2\%$. Conceivably, the parameters d'_{hex} , d_{int} and f_{hex} presented a significant fit correlation. Despite this fact, d_{int} turned out to be of the correct order of magnitude when compared to theoretical studies on the S–Au bond and previous literature on related systems.⁴²

The comparison between data and EMA calculations (dashed thin curves) is presented in Figures 8 and 9. The introduction of the interface model improved the fit, confirming the effectiveness of the Arwin model and the need for a more realistic optical model of the S–Au interface.

This issue was addressed in ref 42, which presented in situ visible SE experiments on *n*-alkanethiol monolayers on a gold substrate immersed in methanol. In the paper, the SAM thickness derived from an ambient/SAM/Au model was found to be systematically underestimated by an amount of about 0.1 nm, with respect to the values obtained with a four-phase (ambient/SAM/interface/Au) model.⁴² Within the four-phase model, the interface dielectric properties were modeled with a Kramers–Kronig consistent set of Lorentzian oscillators, and two SAM-induced transitions in the optical range were claimed.

We did not succeed in resolving these transitions; on a more general ground, any attempt to simulate oscillators, even out of the optical range, collided with severe problems of correlation among the parameters and was finally discarded.

As will be discussed in more detail in the next section, the thickness derived from spectroscopic ellipsometry measurements nicely agrees with the values expected for highly packed SAMs.

Concerning azurin, a first reproduction of data and a reasonable estimate of thickness can be obtained by a simple SAM/Au model, with the organic layer described by a Cauchy model.²⁰ The best fit, obtained with $A = 1.47 \pm 0.01 \times 10^{-3}$, $B = 1.1 \pm 0.4 \times 10^{-3} \mu\text{m}^2$, and $d_{\text{az}} = 3.23 \pm 0.02$ nm, is represented by a dotted curve.

In regard to the azurin layer, results of the interface properties were less critical, and the Arwin EMA model produced only a slight fit improvement, with $d'_{\text{az}} = 3.1 \pm 0.02$ nm, $d_{\text{int}} = 0.10 \pm 0.02$ nm, and $f_{\text{az}} = 92 \pm 2\%$.

In this case, the assumption of perfect transparency involved in the Cauchy approximation seems not fully justified. Photoabsorption measurements in solution shows, in fact (data not shown), absorption bands at 1.97⁴³ and 4.51 eV,⁴⁴ due to the S(Cys-σ) → Cu charge-transfer transition and to electronic transitions originated from UV light absorption of aromatic residues of the protein, respectively.

We therefore attempted a model including absorption features. Absorption was modeled through the introduction of Lorentz oscillators.²⁴ Guided by photoabsorption measurements, we looked for the presence of oscillators in the energy regions corresponding to the absorption bands. The best fit was obtained

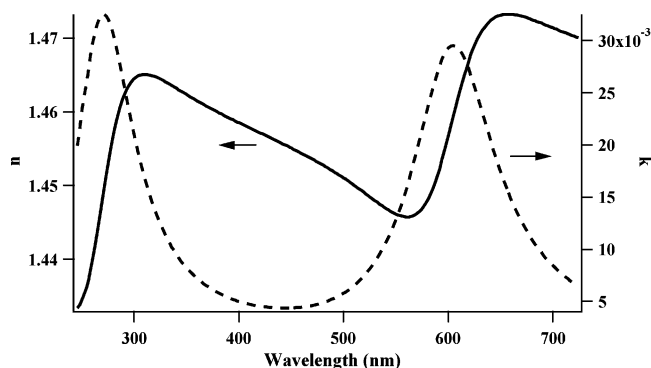


Figure 10. Optical constants for azurin, obtained with Lorentz model.

with two oscillators at energies $E_1 = 2.06 \pm 0.01$ eV and $E_2 = 4.6 \pm 0.2$ eV and $d_{\text{az}} = 3.33 \pm 0.02$ nm. The energy dependence of the optical constants n and k obtained with this model is shown in Figure 10.

With the introduction of the Lorentz oscillators, the data fitting, especially Ψ , definitely improved. However, the value of thickness, mainly related to the variation in the Δ parameter, is close to the value found within the Cauchy approximation. This fact encourages a substantial confidence in our determination of thickness.

Again, the reported uncertainty indicates the 90% level of confidence. The model and fit uncertainties on thickness are therefore smaller than the uncertainty related to the dispersion of measurements, which could be estimated as ± 0.2 nm.

As it concerns the azurin layer grown on predeposited C16, a three-phase model (Azu/C16/Au) was considered. The index of refraction of C16 and azurin layers as well as the thickness of the C16 layer were set to the values found in the analysis of the individual films. In this way, the thickness of the azurin overlayer d_{az}^* remained the only variable to be determined through comparison between calculations and data. We obtained $d_{\text{az}}^* = 2.73 \pm 0.01$ nm. On the basis of this result, SE provides a thickness of the azurin/C16 layer of 4.8 ± 0.2 nm.

5. Discussion

EIS and SE are analytic methods which give independent information on dielectric and packing properties of ultrathin layers. In fact, SE and EIS probe the dielectric properties in two different wavelength ranges: While SE works in the optical region, EIS explores the region from microwaves down to the continuum limit. A close comparison between the EIS and SE results requires a few remarks. First, one has to note that the ellipsometric thickness represents an effective value, resulting from the true layer thickness, due to the molecular orientation and packing, and from the actual coverage. Furthermore, specifically regarding this work, one has to consider that EIS measurements were performed in liquid, while SE measurements were performed *ex situ* in air. The different environments make the comparison between the results of the two techniques less direct, especially regarding the dielectric properties. Nevertheless, information coming from the two techniques can be advantageously combined, gaining in complementarity, cross-consistency, and in-depth comprehension. This possibilities appear particularly useful to control protein coverage and orientation in systems of increasing complexity, formed by SAMs with different functional end groups. As will be discussed later, the combination of EIS and SE results played a decisive role in the interpretation of the data obtained on the azurin/C16 system. Before addressing this system, let us discuss the individual systems. In regard to the C16 SAMs, EIS gave an ϵ_1

value of 2.35 ± 0.1 . SE provided a refractive index n_{hex} of 1.48 ± 0.02 corresponding, for this transparent sample, to ϵ_1 values in the 2.13–2.25 range. The EIS and SE values appear fully compatible, also in view of the different frequency ranges probed by the two methods. These values are generally consistent with the value of 2.25–2.3 reported for polyethylene and with values found for liquid alkanes ($\epsilon_1 \approx 2.1$ –2.2).⁴⁷ The thickness and coverage values obtained by EIS are slightly lower than the ellipsometric thickness (yet compatible within experimental uncertainties) and in overall agreement with results reported in the literature. In particular, the value found for the ellipsometric thickness is in agreement, well within experimental uncertainty, both with early single wavelength ellipsometry results^{48,49} and with more recent determinations with optical⁴² and infrared spectroscopic ellipsometry.⁵⁰ In addition, the thickness values we obtain are in good agreement with a thickness of 2 nm expected for highly packed all-trans molecular chains tilted 30° with respect to the surface normal with an S–Au bond length of 0.19 nm.⁴¹

As it concerns the azurin layer, EIS and SE provide an estimate of the protein dielectric constant in two different environments, in the hydrated and dry states, respectively. EIS gave an ϵ_1 value of 2.85, larger than the value which could be inferred from the n and k values derived from SE (see Figure 10), which are closer to those found in the case of other proteins by means of SE.⁵¹ The difference in the dielectric constant values obtained by the two techniques can be reasonably explained by the two following reasons. First, the two techniques probe the sample properties in two different frequency ranges. Second, the experiments are performed in different environments. The difference in the contacting phase can reasonably account for the azurin higher permittivity found by EIS, because the protein has both hydrophobic and hydrophilic groups which result in a more hydrated system.^{52–54} We note that, remarkably, analysis of SE data suggests the occurrence in the protein layer of absorption bands closely related to the absorption features of free protein in solution. The presence of an absorption band around 600 nm would support the formation of a protein layer in which azurin retains at least part of its functional properties.

The comparison between EIS and SE becomes somewhat more direct concerning the layer thickness. The two sets of measurements suggest a thickness on the order of 3 nm, a factor of 2 larger than recent determinations.²⁰ In this respect, we consider a rough model in which the protein is thought to be a cylinder with a diameter of about 3 nm and a height of about 4 nm.⁵⁵ In this model, the disulfide bridge and the copper ion are located oppositely along the cylinder axis. According to this model, a thickness of about 4 nm is expected for a full-coverage azurin monolayer formed by proteins oriented with the disulfide bridge bound to the gold surface. Our data indicate, therefore, the formation of a quite dense layer with a possible slight tilt of the molecular axis. This result is confirmed by the STM analysis of the azurin/gold interface which shows a fairly uniform distribution of protein molecules with intermolecular distances ranging from 3 to 4 nm (Figure 2).

Furthermore, the thickness/coverage values obtained by EIS are 20% lower than the ellipsometric thickness. This finding suggests that the phase probed by EIS possesses a minor layer density possibly due to minor differences in the self-assembly procedures adopted for the two kinds of measurements. A slightly longer air exposure of the bare gold substrates in EIS measurements due to the cell mounting procedure could account for the observed differences in the thickness/coverage values. Variable coverages, depending on the specific deposition

TABLE 1: Electrical and Structural Parameters of the Self-Assembled Monolayers on Gold Electrode^a,

monolayer	$d_1(\text{nm})$ EIS	ϵ_1 EIS	$d_1(\text{nm})$ SE
hexadecanethiol	2.3 ± 0.2	2.35 ± 0.10	2.1 ± 0.2
azurin	3.2 ± 0.2	2.85 ± 0.20	3.2 ± 0.2
azurin/hexadecanethiol	$2.9^b \pm 0.2$	2.50 ± 0.20	4.8 ± 0.2

^a Derived from EIS and SE measurements. Mean values obtained from different measurements (generally, from 4 to 6 for EIS and 10 for SE) ^b Raw value: apparent thickness obtained from a rough model which actually underestimates the layer thickness. See discussion for the appropriate data analysis.

conditions, have also been reported by Ulstrup and co-workers.¹⁶ However, in both EIS and SE experiments, we obtain films with higher thickness/coverage values compared to the results previously reported for azurin layers deposited on bare gold and functionalized silicon where an effective thickness of 1.5–1.9 nm is observed.²⁰

As far as azurin/C16 SAMs are concerned, whereas the ellipsometric thickness tends to approach the value $d_{\text{hex}}^{\text{SE}} + d_{\text{az}}^{\text{SE}}$ that one should expect on the basis of the measured thickness of the individual layers, the apparent layer thickness derived from EIS data is much lower. This large discrepancy requires a more critical analysis, because for a layered structure, the apparent thickness d_{app} measured in EIS is related to the electrical conductivities of the single layers. In fact, in the case of the composite layer, the equivalent capacitance per unit surface can be modeled as a series of two capacitances, and is given by

$$\frac{\epsilon_{\text{az/hex}}}{d_{\text{app}}} = \frac{d_{\text{az}}^* \epsilon_{\text{az}} \sigma_{\text{hex}}^2 + d_{\text{hex}} \epsilon_{\text{hex}} \sigma_{\text{az}}^2}{(\sigma_{\text{hex}} d_{\text{az}}^* + \sigma_{\text{az}} d_{\text{hex}})^2} \quad (13)$$

where ϵ_{az} , ϵ_{hex} and σ_{az} , σ_{hex} are the permittivities and conductivities of azurin and C16, respectively; d_{az}^* and d_{hex} are the thicknesses of their corresponding layers. The coupling of the information on thickness given by SE with the EIS dielectric characterization opens the route to an estimate of the ratio between the electrical conductivities of the two layers. The values of ϵ_{hex} and ϵ_{az} can be reasonably approximated by the values determined for the individual layers (cf. Table 1). If we now assume an azurin layer conductivity that is 1 order of magnitude higher than the C16 conductivity, inserting for d_{hex} and d_{az}^* the actual thickness values for the individual layers obtained in the SE analysis of the composite system, we obtain an equivalent bilayer thickness $d_{\text{app}} = 2.85$ nm, very close to the value reported in Table 1. Therefore, both EIS and SE, if properly interpreted, give the same thickness value. In fact, the apparent thickness derived from the electrical measurements is exactly the value expected when the composite system is treated as a single effective capacitance whose geometry is obtained by adding the actual thickness of the two component layers. It is indeed reasonable to assume that the metalloprotein layer has a higher conductivity compared to the alkanethiol SAM. Considering the SE results, we note that the thickness of the azurin/C16 layer, $d_{\text{az/hex}}$, is somewhat lower than the sum of the thicknesses of the two layers, $d_{\text{hex}} + d_{\text{az}}$. This result indicates that the ellipsometric thickness of the azurin layer on the C16 SAM, d_{az}^* , is smaller than the thickness of the azurin layer on gold, d_{az} . This means that azurin deposited on a C16 SAM forms a less dense layer compared to the layer formed by self-assembly on bare gold. In turn, the layer density is correlated to the molecular orientation. While on bare gold the disulfide bridge on the outer protein shell constitutes a preferential adsorption

site, on the hydrophobic C16 outer interface, we expect a preferential orientation of the protein with the hydrophobic region near the Cu site pointing toward the C16 surface.¹⁷ A different molecular orientation as well as a less efficient azurin/C16 coupling through the hydrophobic interaction with respect to the disulfide/gold coupling could account for the lower thickness found for the azurin layer when the protein is adsorbed on C16 compared to the deposition on bare metal. The formation of a submonolayer azurin film on alkanethiol SAMs was observed also in the case of azurin deposition on mercaptoacid-coated gold surfaces.¹⁹ Indeed, AFM inspection revealed the presence of a fairly uniform distribution of proteins, either isolated or organized in small clusters, with an average protein height of about 4 nm.

In conclusion, we have reported on a comparative EIS and SE study on azurin, alkanethiol, and azurin/alkanethiol SAMs. The two techniques can be usefully combined to obtain electrical and optical characterization of complex organic layers on solid substrates. The determination of protein dielectric constants is a topic of general interest which is important for theoretical studies⁵⁶ and molecular dynamics simulations⁵⁷ of the protein structure as well as for the investigation of electrostatics-driven key biological phenomena which take place in the interior of proteins such as photoactivation or H^+ and e^- conduction.^{58–60} Moreover, the determination of the protein dielectric constant has recently gained new attention in relation to studies about the functional role of channel proteins.²⁸

Acknowledgment. The authors thank A. Desideri for providing azurin cDNA, E. Cosulich for its expression and purification, F. Gatti for the use of an evaporation chamber, and C. Canale for assistance in gold substrate preparation. This project has been partly financed by Genoa and Rome Universities. Grants from FIRB project Molecular Nano-Devices and MIUR contract 2003028141-005 are also acknowledged.

References and Notes

- (1) Ulman, A. *An introduction to ultrathin organic film: from Langmuir–Blodgett to self-assembly*; Academic Press: Boston, 1991.
- (2) Ciferri, A. *Supramolecular Polymers 2*; Marcel Dekker: New York, 2004.
- (3) Flink, S.; van Veggel, F. C. J. M.; Reinhoudt, D. N. *Adv. Mater. (Weinheim)* **2000**, *12*, 1315–1328.
- (4) Stora, T.; Hovius, R.; Dienes, Z.; Pachoud, M.; Vogel, H. *Langmuir* **1997**, *13*, 5211–5214.
- (5) Kane, R. S.; Takayama, S.; Ostuni, E.; Ingber, D. E.; Whitesides, G. M. *Biomaterials* **1999**, *20*, 2363–2376.
- (6) Cavalleri, O.; Vignolo, M.; Strano, G.; Natale, C.; Rolandi, R.; Thea, S.; Prato, M.; Gonella, G.; Canepa, M.; Gliozzi, A. *Bioelectrochem. Bioenerg.* **2004**, *63*, 3–7.
- (7) Zhang, J.; Grubb, M.; Hansen, A. G.; Kuznetsov, A. M.; Boisen, A.; Wackerbarth, H.; Ulstrup, J. *J. Phys.: Condens. Matter* **2003**, *15*, S1873–S1890.
- (8) Davis, J. J.; Allen, H.; Hill, O. *Chem. Commun.* **2002**, *5*, 393–401.
- (9) Bonanni, B.; Alliata, D.; Bizzarri, A. R.; Cannistraro, S. *Chem-PhysChem* **2003**, *4*, 1183–1188.
- (10) Andolfi, L.; Canters, G. W.; Verbeet, M. P.; Cannistraro, S. *Biophys. Chem.* **2004**, *107*, 107–116.
- (11) Lahiri, J.; Isaacs, L.; Tien, J.; Whitesides, G. M. *Anal. Chem.* **1999**, *71*, 777–790.
- (12) Terrettaz, S.; Stora, T.; Duschl, C.; Vogel, H. *Langmuir* **1993**, *9*, 1361–1369.
- (13) Disley, D. M.; Cullen, D. C.; You, H.; Lowe, C. *Biosens. Bioelectron.* **1998**, *13*, 1213–1225.
- (14) Firestone, M. A.; Shank, M. L.; Sligar, S. G.; Bohn, P. W. *J. Am. Chem. Soc.* **1996**, *118*, 9033–9041.
- (15) Cornell, B. A.; Braach-Maksvytis, V. L. B.; King, L. G.; Osman, P. D. J.; Raguse, B.; Wleczorek, L.; Pace, R. J. *Nature* **1997**, *387*, 580–583.
- (16) Chi, Q.; Zhang, J.; Nielsen, J. U.; Friis, E. P.; Chorkendorff, I.; Canters, G. W.; Andersen, J. E. T.; Ulstrup, J. *J. Am. Chem. Soc.* **2000**, *122*, 4047–4055.

- (17) Gaigalas, A. K.; Niaura, G. *J. Colloid Interface Sci.* **1997**, *193*, 60–70.
- (18) Rinaldi, R.; Biasco, A.; Maruccio, G.; Cingolani, R.; Alliata, D.; Andolfi, L.; Facci, P.; De Rienzo, F.; Di Felice, R.; Molinari, E. *Adv. Mater.* **2002**, *14*, 1453–1457.
- (19) Cavalleri, O.; Natale, C.; Stroppolo, M. E.; Relini, A.; Cosulich, E.; Thea, S.; Novi, M.; Gliozzi, A. *Phys. Chem. Chem. Phys.* **2000**, *2*, 4630–4635.
- (20) Schnyder, B.; Kotz, R.; Alliata, D.; Facci, P. *Surf. Interface Anal.* **2000**, *34*, 40–44.
- (21) Ermolina, I.; Lewis, A.; Feldman, Y. *J. Phys. Chem. B* **2003**, *107*, 14537–14544.
- (22) Terrettaz, S.; Mayer, M.; Vogel, H. *Langmuir* **2003**, *19*, 5567–5569.
- (23) Bordi, F.; Cametti, C.; Gliozzi, A. *Bioelectrochem. Bioenerg.* **2002**, *57*, 39–46.
- (24) Azzam, R. M. A.; Bashara, N. M. *Ellipsometry and polarized light*; North-Holland: Amsterdam, 1977.
- (25) Arwin, H. *Thin Solid Films* **1998**, *313–314*, 764–774.
- (26) Keddie, J. L. *Curr. Opin. Colloid Interface Sci.* **2001**, *6*, 102–110 and reference therein.
- (27) Dwyer, J. J.; Gittis, A. G.; Karp, D. A.; Lattman, E. E.; Spencer, D. S.; Stites, W. E.; García-Moreno, B. *Biophys. J.* **2000**, *79*, 1610–1620.
- (28) Ahern, C. A.; Horn, R. *Trends Neurosci.* **2004**, *27*, 303–307.
- (29) Woollam, J. A.; Johs, B.; Herzinger, C. M.; Hilfiker, J.; Synowicki, R.; Bungay, C. L. *Crit. Rev. Opt. Sc. Technol.* **1999**, *CR72*, 1–28.
- (30) Aspnes, D. E.; Kinsbron, E.; Bacon, D. D. *Phys. Rev. B* **1980**, *21*, 3290–3299.
- (31) Kooij, E. S.; Wormeester, H.; Brouwer, E. A. M.; van Vroonhoven, E.; van Silfhout, A.; Poelsema, B. *Langmuir* **2002**, *18*, 4401–4413 and references therein.
- (32) Sirtori, V.; Magagnin, L.; Saglia, E.; Cavallotti, P. L. *Surf. Sci.* **2004**, *554*, 119–124.
- (33) Gonella, G.; Cavalleri, O.; Emilianov, I.; Mattera, L.; Canepa, M.; Rolandi, R. *Mater. Sci. Eng. C* **2002**, *22*, 359–366.
- (34) Pizzitutti, F.; Bruni, F. *Rev. Sci. Instrum.* **2001**, *72*, 2502–2504.
- (35) Feldman, Y.; Polygalov, E.; Ermolina, I.; Polevaya, Y.; Tsentsiper, B. *Meas. Sci. Technol.* **2001**, *12*, 1355–1364.
- (36) Bordi, F.; Cametti, C.; Gili, T. *Bioelectrochem. Bioenerg.* **2001**, *54*, 53–61.
- (37) Grant, E. H.; Sheppard, R. J.; South, G. P. *Dielectric behaviour of biological molecules in solutions*; Clarendon Press: Oxford, 1978.
- (38) Schreiber, F. *Prog. Surf. Sci.* **2000**, *65*, 151–257.
- (39) Martensson, J.; Arwin, H. *Langmuir* **1995**, *11*, 963–968.
- (40) Bruggeman, D. A. G. *Ann. Phys.* **1935**, *24*, 636–664.
- (41) Di Felice, R.; Selloni, A.; Molinari, E. *J. Phys. Chem. B* **2003**, *107*, 1151–1156.
- (42) Shi, J.; Hong, B.; Parikh, A. N.; Collins, R. W.; Allara, D. L. *Chem. Phys. Lett.* **1995**, *246*, 90–94.
- (43) Webb, M. A.; Kwong, C. M.; Loppnow, G. R. *J. Phys. Chem. B* **1997**, *101*, 5062–5069.
- (44) Cantor, C. R.; Schimmel, P. R. *Biophysical Chemistry. Part II: Techniques for the study of biological structure and function*; W. H. Freeman and Company: New York, 1980.
- (45) Lanza, V. L.; Herrman, D. B. *J. Polym. Sci.* **1958**, *28*, 622–625.
- (46) Swalen, J. D.; Santo, R.; Take, M.; Fischer, J. *IBM J. Res. Dev.* **1977**, *21*, 169–175.
- (47) Dilger, J. P.; Fisher, L. R.; Haydon, D. A. *Chem. Phys. Lipids* **1982**, *30*, 159–176.
- (48) Bain, C. D.; Troughton, E. B.; Tao, Y.; Evall, J.; Whitesides, G. M.; Nuzzo, R. *J. Am. Chem. Soc.* **1989**, *111*, 321–335.
- (49) Laibinis, P. E.; Whitesides, G. M.; Allara, D. L.; Tao, Y.; Parikh, A. N.; Nuzzo, R. G. *J. Am. Chem. Soc.* **1991**, *113*, 7152–7167.
- (50) Meuse, C. W. *Langmuir* **2000**, *16*, 9483–9487.
- (51) Martensson, J.; Arwin, H.; Nygren, H.; Lundstrom, I. *J. Colloid Interface Sci.* **1995**, *174*, 79–85.
- (52) Israelachvili, J. N. *Intermolecular and surface forces*, 2nd edition; Academic Press: London, 1991.
- (53) Luise, A.; Falconi, M.; Desideri, A. *Proteins: Struct., Funct., Genet.* **2000**, *39*, 56–67.
- (54) Takashima, S. *Electrical properties of biopolymers and membranes*; Adam Hilger: Bristol, 1999.
- (55) Nar, H.; Messerschmidt, A.; Huber, R.; van de Kamp, M.; Canters, G. W. *J. Mol. Biol.* **1991**, *221*, 765–772.
- (56) Gilson, M. K.; Honig, B. H. *Biopolymers* **1986**, *25*, 2097–2019.
- (57) Löffler, G.; Schreiber, H.; Steinhauser, O. *J. Mol. Biol.* **1997**, *270*, 520–534.
- (58) Lee, Y. S.; Krauss, M. *J. Am. Chem. Soc.* **2004**, *126*, 2225–2230.
- (59) Olkhova, E.; Hutter, M. C.; Lill, M. A.; Helms, V.; Michel, H. *Biophys. J.* **2004**, *86*, 1783–1789.
- (60) Sokerina, E. V.; Ullmann, G. M.; van-Pouderoyen, G.; Canters, G. W.; Kostic, N. M. *JBIC, J. Biol. Inorg. Chem.* **1999**, *4*, 111–121.